JOURNAL OF THERMOPHYSICS AND HEAT TRANSFER
Vol. 9, No. 4, October–December 1995

Surface Length Scale Contributions to the Directional and Hemispherical Emissivity and Reflectivity

Yongqing Yang* and Richard O. Buckius†
University of Illinois at Urbana–Champaign, Urbana, Illinois 61801

Rigorous electromagnetic scattering solutions, based on the extinction theorem, are used to investigate the surface geometry contributions to the directional and hemispherical emissivity and to the directional hemispherical reflectivity for one-dimensional configured or random rough surfaces with different material properties. The surface parameters that affect the scattered energy are the surface geometrical shape, including the ratio of transverse length scale over wavelength τ/λ and height over wavelength σ/λ, and the optical properties of the surface material. Through numerical calculations, the dominant contribution to these surface radiative properties is shown to be the slope of the surface, expressed by σ/τ. For a surface consisting of multiple-length scales with different slopes, the subscale with a larger slope is shown to dominate the surface radiative properties of the surface.

Nomenclature

E	=	electric field intensity
F	=	electric field intensity derivative
f	=	real implicit function
G	=	Green's function
H	=	magnetic field intensity
$\boldsymbol{K}, \boldsymbol{k}$	=	wave vector
L	=	magnetic field intensity derivative
L_x	=	surface length
n	=	refractive index
r	=	scattering reflection function
x, z, x', z'	=	surface coordinates
ε	=	permittivity
ζ	=	surface interface
θ	=	angle
κ	=	absorption index
λ	=	wavelength of incident energy
ρ'', ρ'	=	bidirectional reflection function, directional hemispherical reflectivity
σ	=	surface height
τ	=	surface transverse length
τ'', τ'	=	bidirectional transmission function, directional hemispherical transmission
Ω	=	solid angle

Subscripts

s	=	scattered
TE	=	transverse electric polarization
TM	=	transverse magnetic polarization
t	=	transmitted
x, y	=	coordinates
ε	=	medium
λ	=	spectral
0	=	incident, free space

Superscripts

$'$	=	directional, derivative
$''$	=	bidirectional
$>$	=	above
$<$	=	below

Received Nov. 23, 1994; revision received March 27, 1995; accepted for publication April 17, 1995.

*Graduate Research Assistant, Department of Nuclear Engineering.

†Professor, Department of Mechanical and Industrial Engineering. Associate Fellow AIAA.

Introduction

DIRECTIONAL emissivity from a material surface is an important radiative quantity in many thermal engineering problems. Besides the spectrally selective surfaces,[1–4] the construction of directional selective surfaces is also desired in many radiative heat transfer applications. The material properties are the major contributors to spectral selectivity, whereas the geometrical length scales of a surface play an important role in determining the directional selectivity of the surface. The specific surface geometry, described by the transverse length scale over wavelength τ/λ, height over wavelength σ/λ, and specific surface geometrical shape, determines the angular distribution of scattered energy.[5–7] Material properties of the surface, expressed in terms of the optical constants n and κ, affect the magnitude of the scattered energy distribution. For a surface composed of multiple-length scale substructures (see Fig. 1), a single set of surface parameters is not adequate for a complete geometrical description and multiple-length scales are needed. Accurate quantification of the contributions of the substructures to the distribution of scattered energy from the single and multiple-length scale surfaces is important in the understanding of the scattering phenomenon from such surfaces.[8]

Recent works have extended the study for surface structure that is large relative to the wavelength to the surface structure that is of the order of the wavelength.[5–8] These studies of configured surfaces and perfectly conducting random rough surfaces show the important effects of surface length scales, as well as the contributions of surface material properties, on the distribution of scattered energy from the surface. References 5 and 6 present averaged results over incident angles, where the bidirectional reflection function for a positive incident angle is averaged with the negative incident angle of the same amplitude. The incident angle is from -90 to $+90$ deg as defined in Fig. 1a, where an incident angle is considered positive when counting from z axis counterclockwise and negative when clockwise. Only symmetric V-groove surfaces are studied in the work of Ref. 7. For multiple-length scale surfaces, only perfectly conducting random rough surfaces are considered in Ref. 8.

This work presents and generalizes the surface geometrical contributions to directional and hemispherical emissivities and reflectivities. Based on the extinction theorem,[9] the rigorous

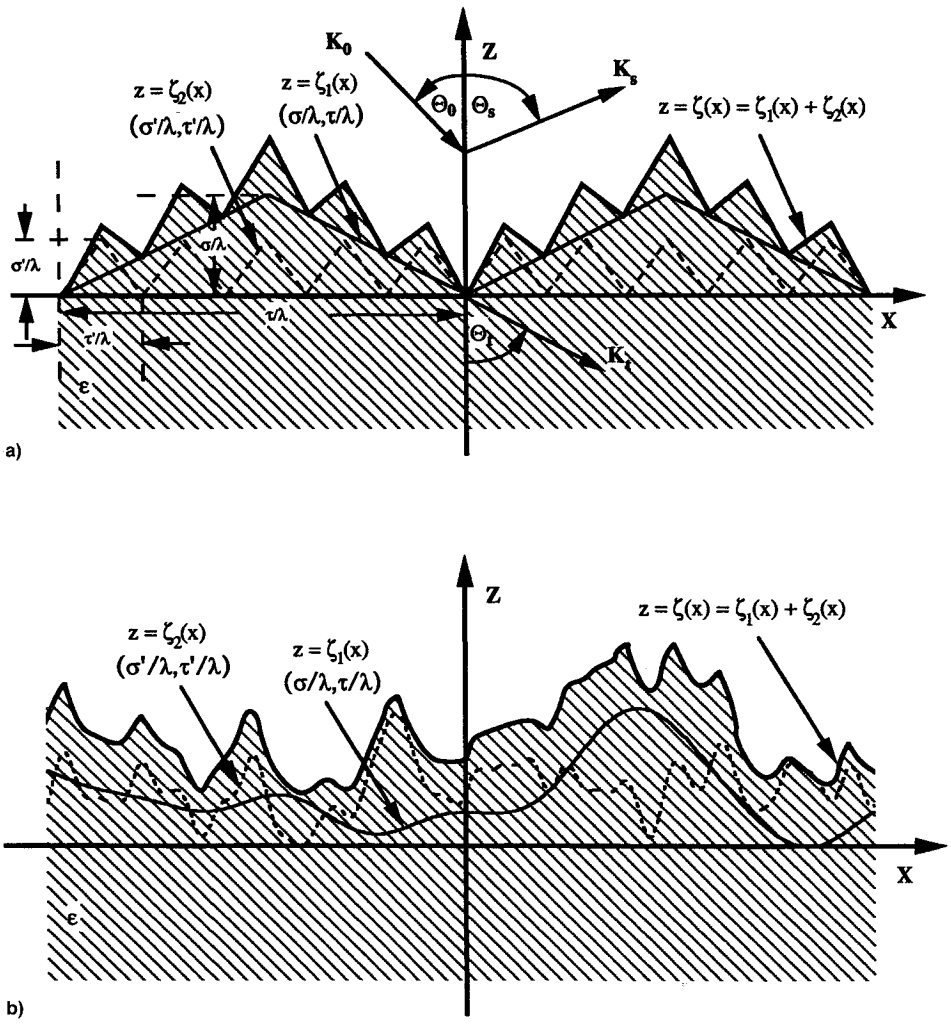

Fig. 1 a) Triangular and b) random multiple-length scale surface profile parameters.

electromagnetic scattering solutions are obtained for different material properties with both configured and random profiles. The following section briefly outlines the theoretical formulation for rigorous electromagnetic scattering solutions. The contributions of the surface geometrical length scales to the directional and hemispherical emissivities and reflectivities are then presented, where surfaces with a single-length scale are studied, followed by the discussion of surfaces with multiple-length scales.

Formulation

A brief development of the electromagnetic theory is given below, with more detailed formulation presented in Refs. 5, 6, and 10. The basic quantities in thermal radiation calculations are the bidirectional reflection function $\rho''_\lambda(\theta_0, \theta_s)$ and the bidirectional transmission function $\tau''_\lambda(\theta_0, \theta_t)$. For a given incident angle θ_0, integration of $\rho''_\lambda(\theta_0, \theta_s)$ over all scattered angles θ_s yields the directional hemispherical reflection $\rho'_\lambda(\theta_0)$ and the integration of $\tau''_\lambda(\theta_0, \theta_t)$ over all transmitted angles θ_t yields the directional hemispherical transmission $\tau'_\lambda(\theta_0)$. For materials with nonzero absorption index, the transmission is zero for infinite medium. From conservation of energy and Kirchhoff's law, the sum of the reflectivity and the emissivity equals unity. Thus, the directional emissivity is related to the directional hemispherical reflection as

$$\varepsilon'_\lambda(\theta_0) = 1 - \rho'_\lambda(\theta_0) = 1 - \frac{1}{\pi}\int_{2\pi} \rho''_\lambda(\theta_0, \theta_s)\cos(\theta_s)\, d\Omega_s \quad (1)$$

Based on the extinction theorem, the rigorous electromagnetic scattering theory gives the bidirectional reflection functions, for TM and TE polarizations, respectively, as

$$\rho''_{\lambda\,\mathrm{TM}}(\theta_0, \theta_s) = \frac{1}{8}\frac{1}{L_x \cos\theta_s \cos\theta_0}|r_{\mathrm{TM}}(\theta_s)|^2 \quad (2a)$$

$$\rho''_{\lambda\,\mathrm{TE}}(\theta_0, \theta_s) = \frac{1}{8}\frac{1}{L_x \cos\theta_s \cos\theta_0}|r_{\mathrm{TE}}(\theta_s)|^2 \quad (2b)$$

where

$$r_{\mathrm{TM}}(\theta_s) = \int_{-\infty}^{\infty} \exp\{-ik_0[x\sin\theta_s + \zeta(x)\cos\theta_s]\} \times \{ik_0[\zeta'(x)\sin\theta_s - \cos\theta_s]H(x) - L(x)\}\, dx \quad (3a)$$

$$r_{\mathrm{TE}}(\theta_s) = \int_{-\infty}^{\infty} \exp\{-ik_0[x\sin\theta_s + \zeta(x)\cos\theta_s]\} \times \{ik_0[\zeta'(x)\sin\theta_s - \cos\theta_s]E(x) - F(x)\}\, dx \quad (3b)$$

where

$$H(x) = H_y^{>}(x, z)|_{z=\zeta(x)} = H_y^{<}(x, z)|_{z=\zeta(x)} \quad (4a)$$

$$L(x) = \left[-\zeta'(x)\frac{\partial}{\partial x} + \frac{\partial}{\partial z}\right] H_y^{>}(x, z)|_{z=\zeta(x)} = \frac{1}{\varepsilon}\left[-\zeta'(x)\frac{\partial}{\partial x} + \frac{\partial}{\partial z}\right] H_y^{<}(x, z)|_{z=\zeta(x)} \quad (4b)$$

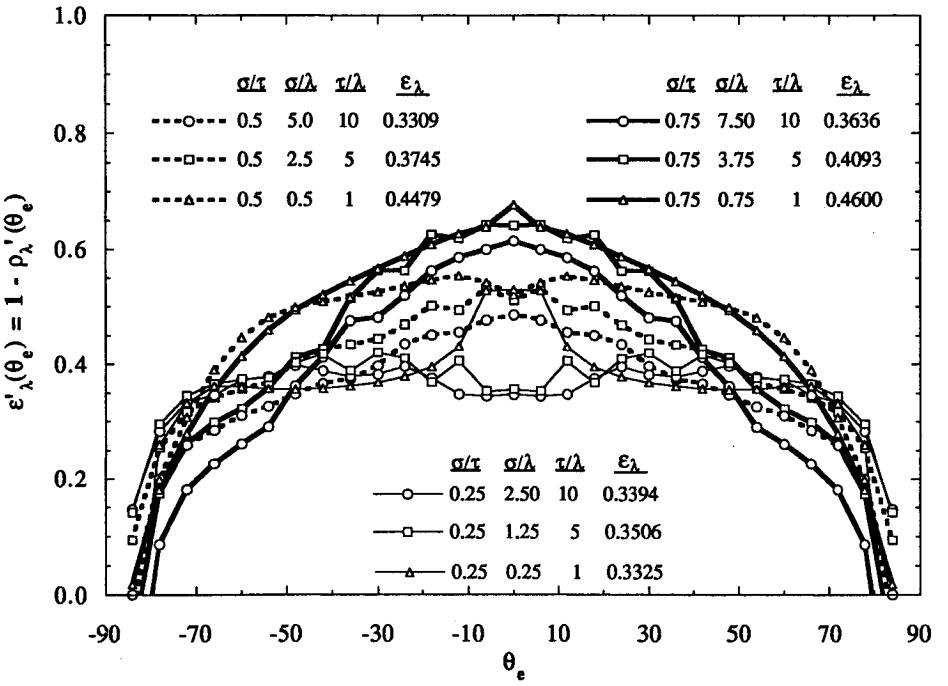

Fig. 2 Directional emissivities from symmetric triangular surfaces, with $n = 2.0$ and $\kappa = 4.0$, and different σ/λ and τ/λ.

$$E(x) = E_y^{>}(x, z)|_{z=\zeta(x)} = E_y^{<}(x, z)|_{z=\zeta(x)} \tag{4c}$$

$$F(x) = \left[-\zeta'(x)\frac{\partial}{\partial x} + \frac{\partial}{\partial z}\right] E_y^{>}(x, z)|_{z=\zeta(x)} = \left[-\zeta'(x)\frac{\partial}{\partial x} + \frac{\partial}{\partial z}\right] E_y^{<}(x, z)|_{z=\zeta(x)} \tag{4d}$$

All symbols are defined in the Nomenclature and surface geometrical parameters are shown in Fig. 1.

The magnetic and electric fields $H(x)$ and $E(x)$ and their derivatives $L(x)$ and $F(x)$ along the surface, defined in Eqs. (4), are determined by Eqs. (5) and (6), as

$$H(x) = H(x)_0 + \frac{1}{4\pi}\int_{-\infty}^{\infty}\left\{H(x')\left[-\zeta'(x')\frac{\partial}{\partial x'} + \frac{\partial}{\partial z'}\right] \times G_0[x, z = z(x), x', z']|_{z'=\zeta(x')} - G_0[x, z = \zeta(x), x', z']L(x')|_{z'=\zeta(x')}\right\} dx' \tag{5a}$$

$$H(x) = \frac{-1}{4\pi}\int_{-\infty}^{\infty}\left\{H(x')\left[-\zeta'(x')\frac{\partial}{\partial x'} + \frac{\partial}{\partial z'}\right] \times G_\varepsilon[x, z = \zeta(x), x', z']|_{z'=\zeta(x')} - \varepsilon G_\varepsilon[x, z = \zeta(x), x', z']L(x')|_{z'=\zeta(x')}\right\} dx' \tag{5b}$$

$$E(x) = E(x)_0 + \frac{1}{4\pi}\int_{-\infty}^{\infty}\left\{E(x')\left[-\zeta'(x')\frac{\partial}{\partial x'} + \frac{\partial}{\partial z'}\right] \times G_0[x, z = \zeta(x), x', z']|_{z'=\zeta(x')} - G_0[x, z = \zeta(x), x', z']F(x')|_{z'=\zeta(x')}\right\} dx' \tag{6a}$$

$$E(x) = \frac{-1}{4\pi}\int_{-\infty}^{\infty}\left\{E(x')\left[-\zeta'(x')\frac{\partial}{\partial x'} + \frac{\partial}{\partial z'}\right] \times G_\varepsilon[x, z = \zeta(x), x', z']|_{z'=\zeta(x')} - G_\varepsilon[x, z = \zeta(x), x', z']F(x')|_{z'=\zeta(x')}\right\} dx' \tag{6b}$$

where $G_\varepsilon(x, z, x', z')$ and $G_0(x, z, x', z')$ are the Green's functions in the medium and the vacuum.

Numerical discretization of Eqs. (5) and (6), over the surface length L_x, leads to a set of numerical simultaneous linear equations.[10] This set of numerical simultaneous linear equations is then solved to obtain the final solutions of $H(x)$, $E(x)$, $L(x)$, and $F(x)$ on the surface, which, in turn, provide the bidirectional reflection functions. The directional emissivity is then obtained from Eq. (1). In the calculations carried out in this study, L_x is chosen as long as computationally possible, ranging from 20λ to 180λ, depending on the value of τ/λ, to minimize the edge effects from the plane incident wave. The number of mesh points along the surface length ranges from 400, for small values of σ/τ, to 2500, for large values of σ/τ. One hundred surface realizations are performed and averaged to obtain all the random rough surface results presented. Energy conservation is examined for nonabsorbing dielectric material properties (i.e., $\kappa = 0.0$). In the calculations for configured surfaces, the energy conservation is maintained within 1% for surfaces with small slopes of σ/τ. For surfaces with large slopes of σ/τ, conservation to within 1% is maintained for incident angles near normal and reduces to 4% for angles larger than 40 deg from the normal. The energy conservation for one surface realization in the random rough surface calculation is between 2–4%, and is reduced to within 1% when averaged over 100 realizations. The calculations are performed on either Cray Y-MP C90 or Convex C3880 supercomputers.

Results

Surfaces with a Single-Length Scale

Surface geometrical parameters shown in Fig. 1, including the transverse length divided by wavelength τ/λ, the height

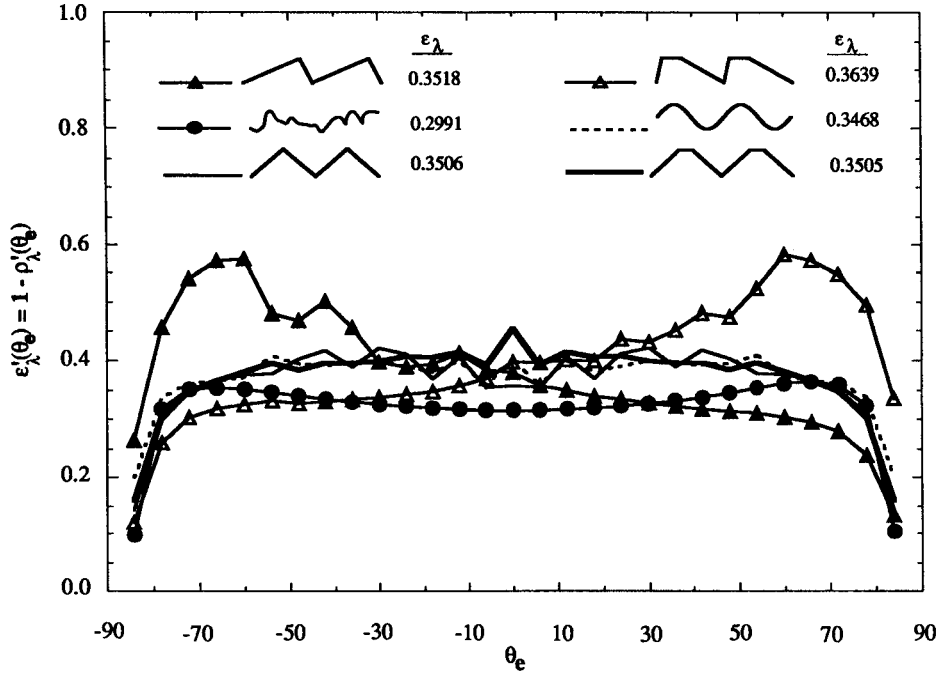

Fig. 3 Directional emissivities from surfaces, with $n = 2.0$ and $\kappa = 4.0$, and different geometrical shapes ($\sigma/\tau = 0.25$; $\sigma/\lambda = 1.25$, $\tau/\lambda = 5.0$).

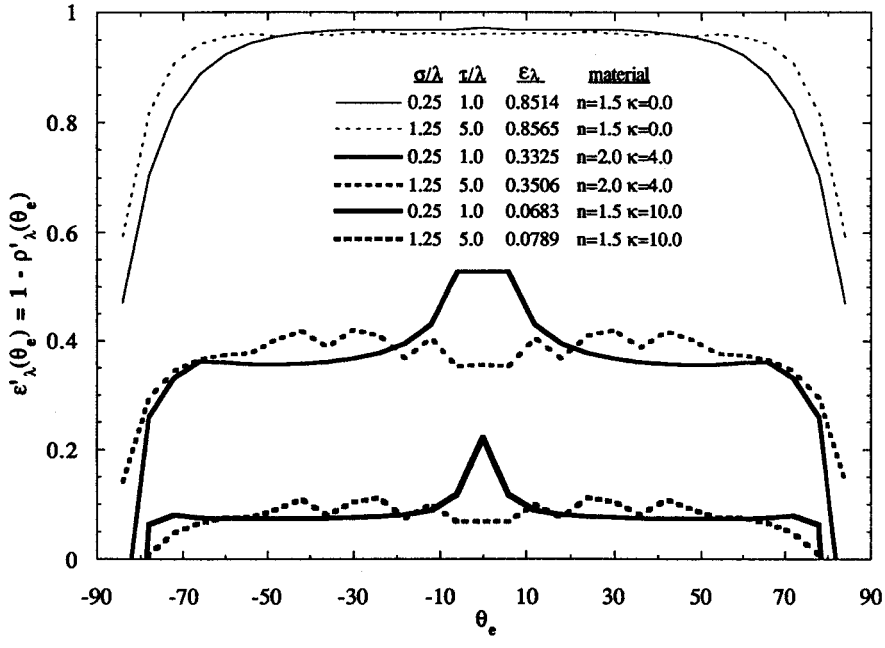

Fig. 4 Directional emissivities from symmetric triangular surfaces of different materials, with a constant ratio of $\sigma/\tau = 0.25$.

divided by wavelength σ/λ, and specific surface geometrical shape affect the directional emissivity, both in magnitude and directional distribution. Consequently, the hemispherical emissivity, which is the integration of the directional emissivity, is also affected. These surface parameters determine the angular distribution of the scattered energy.[5] To generalize the geometry effects on emissivity, a particular triangular geometry for a semiconductor material (Si) with optical constants of $n = 2.0$ and $\kappa = 4.0$ is considered. The ratio of transverse length over wavelength τ/λ ranges from 1.0 to 10.0, and the ratio of height over wavelength σ/λ ranges from 0.25 to 7.5. The surfaces are divided into three groups with constant slopes of σ/τ, from 0.25, 0.5, to 0.75. The emissivities are presented in Fig. 2. The results in Fig. 2 are grouped by constant slope σ/τ, and the directional emissivities show some variation in magnitude and shape, yet the directional emissivity and the hemispherical emissivity are dominated by this slope. Both the directional emissivity and the hemispherical emissivity are not as strongly dependent on the ratio of transverse length over wavelength τ/λ, or the ratio of height over wavelength σ/λ alone, as they are dependent on the slope σ/τ. Thus, this slope is the dominant factor in determining the hemispherical emissivity, while different values of σ/λ and τ/λ yield slightly different directional emissivities. Comparisons between the three groups, each with the same slope, reveal that when the slope is increased, the magnitude in the directional emissivity is increased for small angles around the normal angle and the magnitude of the hemispherical emissivity is also increased. Additional cases with much smaller ratios of σ/τ (as low as 0.05) were also investigated (not shown) and they follow these same trends.

The investigation of the importance of the surface slope is further examined for different geometrical shapes and different materials. A constant slope of σ/τ (σ/τ = 0.25, σ/λ = 1.25, τ/λ = 5.0) is chosen and different geometrical shapes are considered. The emissivities are presented in Fig. 3 for the same semiconductor material with n = 2.0 and κ = 4.0. Six different geometries are considered: a symmetric triangle, a truncated symmetric triangle, an asymmetric triangle, a truncated asymmetric triangle, a sine function surface, and a random rough surface. The methodology for the derivation of analytical expressions for the configured surfaces is given in the Appendix. The generation of the random rough surfaces is also described in the Appendix. For these six geometrical shapes, it is once again observed that the hemispherical emissivities are relatively similar. The extreme change in magnitude is less than 20% when compared with the random rough surface, which has the lowest magnitude among all these six geometries. The hemispherical emissivities for the configured surfaces show a difference of less than 5%. It is noteworthy that the directional emissivity curve for a smooth surface, with n = 2.0 and κ = 4.0, is relatively flat with ε_λ = 0.2987. The result is not shown in the figures for the reason of clarity.

In Fig. 3, however, large variations in the magnitudes of directional emissivities are observed for asymmetrically configured surfaces, the asymmetric triangle and the truncated asymmetric triangle. The directional variation can be a factor of 2 in magnitude. This shows that, to obtain directional selective emissivities, an asymmetric geometry should be cho-

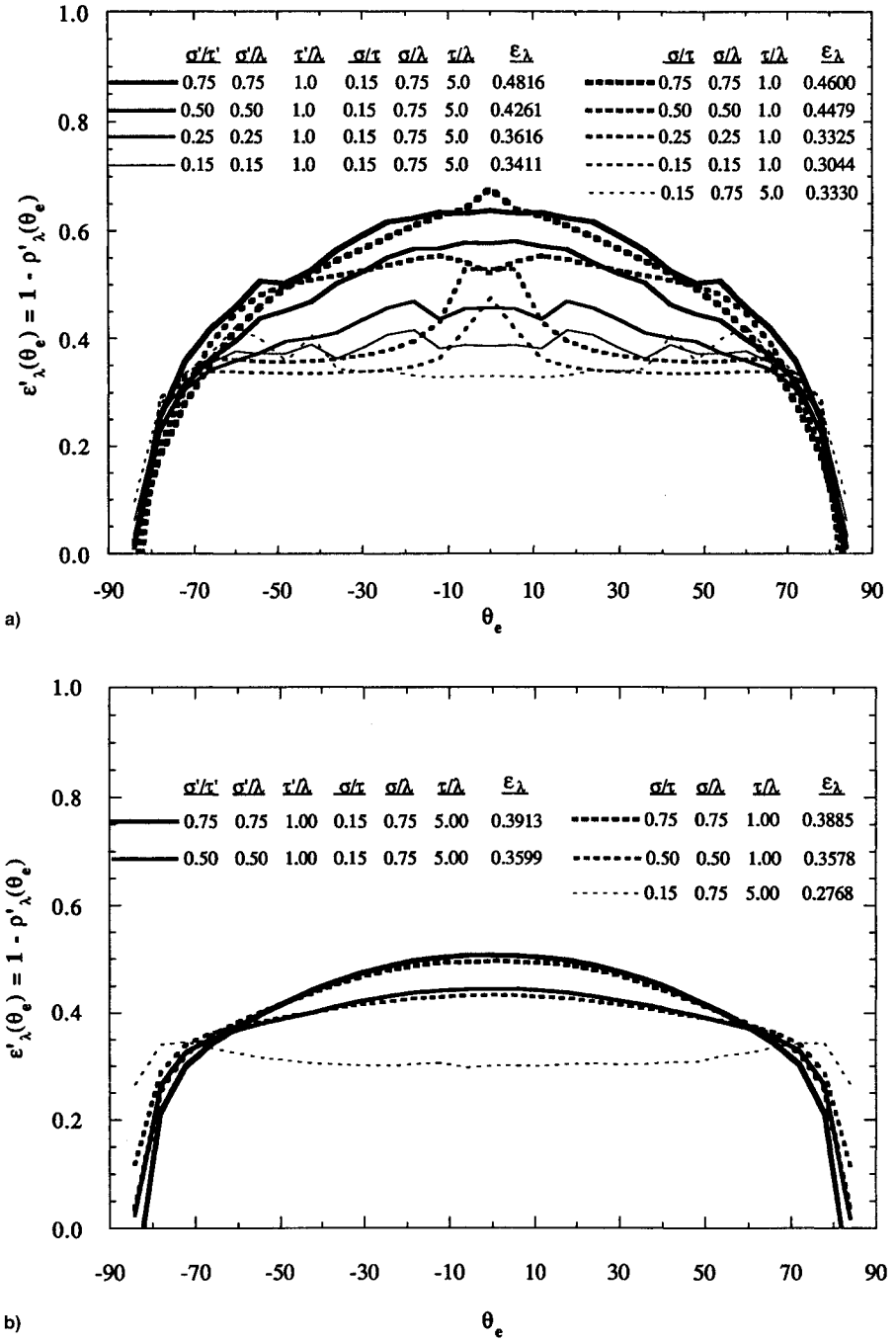

Fig. 5 a) Directional emissivities from symmetric triangular multiple-length scale surfaces, with n = 2.0 and κ = 4.0, where a triangle with σ'/λ and τ'/λ is linearly superimposed onto a triangle with σ/λ and τ/λ and b) directional emissivities from random multiple-length scale surfaces, with n = 2.0 and κ = 4.0, where a random surface with σ'/λ and τ'/λ is linearly superimposed onto another random surface with σ/λ and τ/λ. One hundred surface realizations used in each case.

sen.[2,7] The magnitude of directional emissivity and hemispherical emissivity from random rough surface is less than those from configured surfaces and the directional emissivity from random rough surface is less directionally dependent.

The material used in all the results presented in Figs. 2 and 3 is the same semiconductor material with optical constants of $n = 2.0$ and $\kappa = 4.0$. The effects of geometrical parameters are also examined for a nonabsorbing dielectric material, with optical constants of $n = 1.5$ and $\kappa = 0.0$, and a metal material with $n = 1.5$ and $\kappa = 10.0$. The surfaces are the symmetric triangles with a constant ratio of $\sigma/\tau = 0.25$, and various values of σ/λ and τ/λ. The emissivities are presented in Fig. 4. The magnitudes of the directional and hemispherical emissivity are significantly affected by the material properties. For a specific material, however, the surface slope σ/τ is the dominant factor affecting the hemispherical emissivity and the directional emissivity. This generalizes the observation that, for a given material, the surface slope σ/τ is the dominant factor in determining the hemispherical emissivity and an important factor in quantifying the directional emissivities from surfaces with symmetric or random surface structures. For surfaces with asymmetric geometries shown in Fig. 3, the geometrical shape plays an important role in obtaining directional emissivities.

Surfaces with Multiple Length Scales

The contribution of multiple length scales of a surface to the surface emission and reflection is investigated for a semiconductor material with optical constants of $n = 2.0$ and $\kappa = 4.0$. The surface profiles are either symmetric triangular surfaces or random rough surfaces. A surface profile with σ'/λ and τ'/λ is linearly superimposed on another surface profile with σ/λ and τ/λ. The ratio of σ'/τ' is of the order of σ/τ or larger. The surface profile parameters for triangular surfaces and random rough surfaces are defined in Fig. 1. The directional and hemispherical emissivities from these multiple-length scale surfaces are presented in Fig. 5, together with single-length scale surfaces that are the substructures of the multiple-length scale surfaces. In Fig. 5a, a triangle surface with $\sigma/\tau = 0.15$ ($\sigma/\lambda = 0.75$, $\tau/\lambda = 5.0$) serves as a "base" triangle. Triangles with $\sigma'/\tau' = 0.15$ ($\sigma'/\lambda = 0.15$, $\tau'/\lambda = 1.0$), $\sigma'/\tau' = 0.25$ ($\sigma'/\lambda = 0.25$, $\tau'/\lambda = 1.0$), $\sigma'/\tau' = 0.5$ ($\sigma'/\lambda = 0.5$, $\tau'/\lambda = 1.0$), and $\sigma'/\tau' = 0.75$ ($\sigma'/\lambda = 0.75$, $\tau'/\lambda = 1.0$) are linearly superimposed onto this "base" triangle. Comparing the multiple-length scale surface results to the single-length surface results for both directional and hemispherical emissivities, the dominance of the largest slope is shown. For the triangular surfaces in Fig. 5a, the profile with σ'/τ' larger than σ/τ dominates the radiative properties, even $\sigma'/\lambda < \sigma/\lambda$ and $\tau'/\lambda < \tau/\lambda$. As the substructure geometries become similar, the contributions to the emissivities from the substructures are relatively equal since $\sigma/\tau \approx \sigma'/\tau'$ ($\sigma/\tau = 0.15$, $\sigma'/\tau' = 0.15$ and $\sigma/\tau = 0.15$, $\sigma'/\tau' = 0.25$). Since the slope of the multiple-length scale surface is larger than the slopes of the two individual substructures, the hemispherical emissivity from the multiple-length scale surface is increased when compared with the ones from the two individual substructures, especially the "base" substructure. Thus, when the surface is composed of two substructures with different slopes, the substructure with the larger slope prescribes the directional and hemispherical emissivity, even though the substructure with smaller slope has larger length scales (σ/λ and τ/λ). Random rough semiconductor surfaces results are presented in Fig. 5b, where 100 surface realizations are used in all the cases. As for the triangular surfaces in Fig. 5a, a random rough surface with σ'/λ and τ'/λ is linearly superimposed onto another random rough surface with σ/λ and τ/λ, where $\sigma'/\lambda < \sigma/\lambda$ and $\tau'/\lambda < \tau/\lambda$. Once again, the dominance of the substructure with a larger slope on the directional emissivity and the hemispherical emissivity is observed for the multiple-length scale random rough surfaces.

Conclusions

Using the rigorous electromagnetic theory, the geometrical contributions of one-dimensional material surfaces to the directional emissivity and hemispherical directional reflectivity are investigated. For surfaces with a single-length scale, among all the geometrical parameters that affect the directional emissivity and the hemispherical emissivity, the dominant parameter is the slope of the surface, expressed as the ratio of σ/τ. Both the directional emissivity and the hemispherical emissivity are dominated by the slope of the surface. For a given surface slope, hemispherical emissivities from different surface geometries are similar, with slight variations in directional emissivities for random and symmetrically configured surfaces. Directional emissivities show significant variation in magnitude at different angles for surfaces with asymmetric geometrical shapes. The magnitude of emissivity is found to be dependent on the slope of the surface as well as the optical properties of the surface material. Directional emissivities from random rough surfaces are more uniform than those from configured surfaces of the same surface slope.

Emission from surfaces with multiple-length scales is also investigated. When a surface is composed of two substructures with different length scales, the substructure with larger slope prescribes the radiative properties of the surface. This dominance is diminished when the slopes of the substructures are similar and the contributions from the individual substructures become similar. These trends are valid for both random rough and configured multiple-length scale surfaces.

Appendix: Generation of Surface Profiles

Generation of Configured Surface Profiles

Implicit real functions are used to describe the geometry of rigid solids.[11] Based on the algebra of logic and measure theory, equations are obtained to analytically describe geometrical objects or regions. This concept is applied here to obtain the analytical expressions of surface profiles.

The primitives in the geometrical descriptions are typically half-spaces defined by inequalities $f(x, z) \geq 0$ or $f(x, z) \leq 0$, where $f(x, z)$ are real-valued functions of real variables. Geometrical objects, or regions, are defined through Boolean operations on these primitives. The two basic operations used here are the logic "and" ($\cap$) and logic "or" ($\cup$), which are defined as

$$f_1 \cap f_2 = \min(f_1, f_2) = \tfrac{1}{2}(f_1 + f_2 - |f_1 - f_2|) \geq 0 \quad \text{(A1)}$$

$$f_1 \cup f_2 = \max(f_1, f_2) = \tfrac{1}{2}(f_1 + f_2 + |f_1 - f_2|) \geq 0 \quad \text{(A2)}$$

if $f_1(x, z) \geq 0$, $f_2(x, z) \geq 0$, and

$$f_1 \cap f_2 = \max(f_1, f_2) = \tfrac{1}{2}(f_1 + f_2 + |f_1 - f_2|) \leq 0 \quad \text{(A3)}$$

$$f_1 \cup f_2 = \min(f_1, f_2) = \tfrac{1}{2}(f_1 + f_2 - |f_1 - f_2|) \leq 0 \quad \text{(A4)}$$

if $f_1(x, z) \leq 0$, $f_2(x, z) \leq 0$.

When the geometrical objects, or regions, have more than two primitives, the Boolean operations have to be performed repeatedly to include all the primitives. The equation describing the surface profile is then obtained by taking the equal sign for the final function obtained through the Boolean operation.

As an example, from the three inequality primitives as

$$f_1 = z - (\sigma/\tau_1)x \leq 0, \qquad 0 \leq x \leq \tau_1 \quad \text{(A5a)}$$

$$f_2 = z - \sigma \leq 0, \qquad \tau_1 \leq x \leq \tau_2 \quad \text{(A5b)}$$

$$f_3 = z - [\sigma(\tau - x)/(\tau - \tau_2)] \leq 0, \qquad \tau_2 \leq x \leq \tau \quad \text{(A5c)}$$

the analytical expression for the truncated asymmetric triangle surface profile is

$$z = \frac{\sigma}{2}\left(\mathcal{R} + \frac{1}{9}\frac{\tau - x}{\tau_1} - \left|\mathcal{R} - \frac{1}{9}\frac{\tau - x}{\tau_1}\right|\right) \qquad 0 \le x \le \tau \tag{A6}$$

where

$$\mathcal{R} = \frac{1}{2}\left(1 + \frac{x}{\tau_1}\right) - \frac{1}{2}\left|1 - \frac{x}{\tau_1}\right|, \quad \tau_1 = 0.08\tau, \quad \tau_2 = 0.28\tau \tag{A7}$$

Generation of Random Rough Surface Profiles

This section outlines the generation of random surface profiles. These surfaces are described by a Gaussian distributed stochastic height function, $z = \zeta(x)$, with the following statistical properties:

$$\langle \zeta(x) \rangle = 0 \tag{A8}$$

$$\langle \zeta(x)\zeta(x') \rangle = \sigma^2 \exp\left[\frac{-(x - x')^2}{\tau^2}\right] \tag{A9}$$

where σ^2 is the mean-square departure of the surface height from its zero mean, and τ is the transverse correlation length, which is a measure of the mean distance between consecutive peaks and valleys on the surface.

A random number X_i is generated through the inversion of the integral

$$\frac{1}{\sqrt{2\pi}} \int_{-\infty}^{X_i} \exp\left(-\frac{x^2}{2}\right) dx = R_{X_i} \tag{A10}$$

where R_{X_i} is a random number uniformly chosen from the interval [0, 1]. Random numbers X_i possess a Gaussian distribution without satisfying the property defined in Eq. (A9). Therefore, they do not have the correct rms deviation σ. A digital filter is applied to provide the correct deviation through

$$\zeta(\zeta_k) = \sigma \sum_{j=-M}^{M-1} W_j X_{j+k} \tag{A11}$$

where W_j are the digital filter weights, M is a large integer, and $\zeta(\zeta_k)$ is the surface height at $x = \zeta_k$. The detailed formulation for W_j is found in Ref. 10.

Acknowledgments

This work is supported, in part, by the National Center for Supercomputing Applications, Urbana, Illinois, Pittsburgh Supercomputing Center, Pittsburgh, Pennsylvania, and the Richard W. Kritzer Foundation.

References

[1]Demont, P., Huetz-Aubert, M., and N'Guyen, T. H., "Experimental and Theoretical Studies of the Influence of Surface Conditions on Radiative Properties of Opaque Materials," *International Journal of Thermophysics*, Vol. 3, No. 4, 1982, pp. 335–364.

[2]Granqvist, C. G., "Spectrally Selective Surface Coatings for Energy Efficiency and Solar Applications," *The Physics Teacher*, Vol. 22, Sept. 1984, pp. 372–383.

[3]Modest, M. F., *Radiative Heat Transfer*, McGraw–Hill, New York, 1993, Chap. 3.

[4]Siegel, R., and Howell, J. R., *Thermal Radiation Heat Transfer*, 3rd ed., Hemisphere, Washington, 1992, Chap. 5.

[5]Dimenna, R. A., and Buckius, R. O., "Electromagnetic Theory Predictions of the Directional Scattering from Triangular Surfaces," *Journal of Heat Transfer*, Vol. 116, Aug. 1994, pp. 639–645.

[6]Dimenna, R. A., and Buckius, R. O., "Quantifying Specular Approximations for Angular Scattering from Perfectly Conducting Random Rough Surfaces," *Journal of Thermophysics and Heat Transfer*, Vol. 8, No. 3, 1994, pp. 393–399.

[7]Elich, J. J. Ph., Koppers, G. A. A., and Wieringa, J. A., "The Energy-Saving Effects of Surface-Structured Walls in a Glass-Melting Furnace," *Journal of the Institute of Energy*, Vol. 66, No. 467, 1993, pp. 71–78.

[8]Tsang, L., Chan, C. H., Pak, K., Sangani, H., Ishimaru, A., and Phu, P., "Monte Carlo Simulations of Large-Scale Composite Random Rough-Surface Scattering Based on the Banded-Matrix Iterative Approach," *Journal of the Optical Society of America A*, Vol. 11, No. 2, 1994, pp. 691–696.

[9]Wolf, E., "A Generalized Extinction Theorem and Its Role in Scattering Theory," *Coherence and Quantum Optics*, edited by E. Wolf, Plenum, New York, 1973, pp. 339–357.

[10]Maradudin, A. A., Michel, T., McGurn, A. R., and Mendez, E. R., "Enhanced Backscattering of Light from a Random Grating," *Annals of Physics*, Vol. 203, No. 2, 1990, pp. 255–307.

[11]Shapiro, V., "Real Functions for Representation of Rigid Solids," *Computer Aided Geometric Design*, Vol. 11, 1994, pp. 153–175.